

# IMPROVING DEEP IMAGE MATTING VIA LOCAL SMOOTHNESS ASSUMPTION

Rui Wang<sup>1</sup>, Jun Xie<sup>2\*</sup>, Jiacheng Han<sup>3</sup> and Dezhen Qi<sup>4</sup>

<sup>1</sup>Center for Applied Statistics and School of Statistics,  
Renmin University of China, Beijing 100872, China

<sup>2</sup>PCIE Lab, Lenovo Research, Beijing, China

<sup>3</sup>School of Optics and Photonics, Beijing Institute of Technology, Beijing, China

<sup>4</sup>Department of Physics, and Fujian Provincial Key Laboratory for Soft Functional Materials Research,  
Xiamen University, Xiamen 361005, China

## ABSTRACT

Natural image matting is a fundamental and challenging computer vision task. Conventionally, the problem is formulated as an underconstrained problem. Since the problem is ill-posed, further assumptions on the data distribution are required to make the problem well-posed. For classical matting methods, a commonly adopted assumption is the local smoothness assumption on foreground and background colors. However, the use of such assumptions was not systematically considered for deep learning based matting methods. In this work, we consider two local smoothness assumptions which can help improving deep image matting models. Based on the local smoothness assumptions, we propose three techniques, i.e., training set refinement, color augmentation and backpropagating refinement, which can improve the performance of the deep image matting model significantly. We conduct experiments to examine the effectiveness of the proposed algorithm. The experimental results show that the proposed method has favorable performance compared with existing matting methods.

**Index Terms**— Image matting, backpropagating refinement, data augmentation

## 1. INTRODUCTION

Natural image matting is an important task in image editing. In this task, the natural image  $\mathcal{I}$  is assumed to be a convex combination of the foreground  $\mathcal{F} \in \mathbb{R}^{h \times w \times 3}$  and the background  $\mathcal{B} \in \mathbb{R}^{h \times w \times 3}$  weighted by  $\alpha \in [0, 1]^{h \times w}$ , the opacity of the foreground. Formally, the color at  $i \in \{1, \dots, h\} \times \{1, \dots, w\}$  satisfies the compositing equation

$$\mathcal{I}_i^c = \alpha_i \mathcal{F}_i^c + (1 - \alpha_i) \mathcal{B}_i^c, \quad c = 1, 2, 3. \quad (1)$$

Given an input image  $\mathcal{I}$ , the goal is to estimate  $\alpha$ . Note that there are 3 equations with 7 unknowns at each pixel. This results in the nonidentifiability of  $\mathcal{F}$ ,  $\mathcal{B}$  and  $\alpha$ . Specifically,

suppose that the triplet  $(\mathcal{F}, \mathcal{B}, \alpha)$  satisfies (1). Then for any  $Q \in \mathbb{R}^{h \times w}$  satisfying  $0 \leq Q_i \leq \frac{1}{\alpha_i}$ , the triplet  $((\mathcal{B}_i^c + (\mathcal{F}_i^c - \mathcal{B}_i^c)/Q_i), \mathcal{B}, (Q_i \alpha_i))$  also satisfies (1). Thus, without further assumption, the natural image matting problem is ill-posed.

To regulate the problem, natural image matting is often aided by human. In a typical human-aided process, the user provides a trimap  $\mathcal{T} \in \{0, 0.5, 1\}^{h \times w}$  indicating the purely foreground region  $\{i : T_i = 1\}$ , the purely background region  $\{i : T_i = 0\}$ , and the unknown region  $\{i : T_i = 0.5\}$ . It is guaranteed that if  $T_i = 1$  then  $\alpha_i = 1$  and if  $T_i = 0$  then  $\alpha_i = 0$ . With a trimap  $\mathcal{T}$ , one only needs to estimate  $\alpha$  in the unknown region. However, the compositing equation (1) is still ill-posed in the unknown region. In principle, further assumptions are still required to make the problem well-posed.

For traditional image matting methods, local smoothness assumptions on  $\mathcal{F}$ ,  $\mathcal{B}$  or  $\alpha$  are commonly used. In a seminal work, Levin *et al.* [1] proposed the color line model based on the assumption that  $\mathcal{F}$  and  $\mathcal{B}$  are approximately constant locally. There are also methods which utilize smoothness assumptions on  $\alpha$ ; see [2] and the references therein. For traditional methods, a main goal of imposing local smoothness assumptions is to formulate tractable models. Consequently, their assumptions may be overly strong.

Thanks to the large training data released by Xu *et al.* [3] and the advent of convolutional neural networks, deep learning based matting methods have achieved significantly better performances than traditional methods [3–8]. For deep learning methods, one does not need to formulate an explicit model of colors. Rather, the deep neural networks may learn the implicit local smoothness assumptions during training. Intuitively, deep learning methods may be improved if they are explicitly guided by local smoothness assumptions. Unfortunately, to our best knowledge, no existing deep learning method utilizes the local smoothness assumptions explicitly.

In this paper, we explore the use of local smoothness assumption in deep image matting. We consider two seemingly trivial assumptions that should be satisfied by natural images. Surprisingly, these simple assumptions can be violated by

\*Corresponding author: Jun Xie (xiejun@lenovo.com)

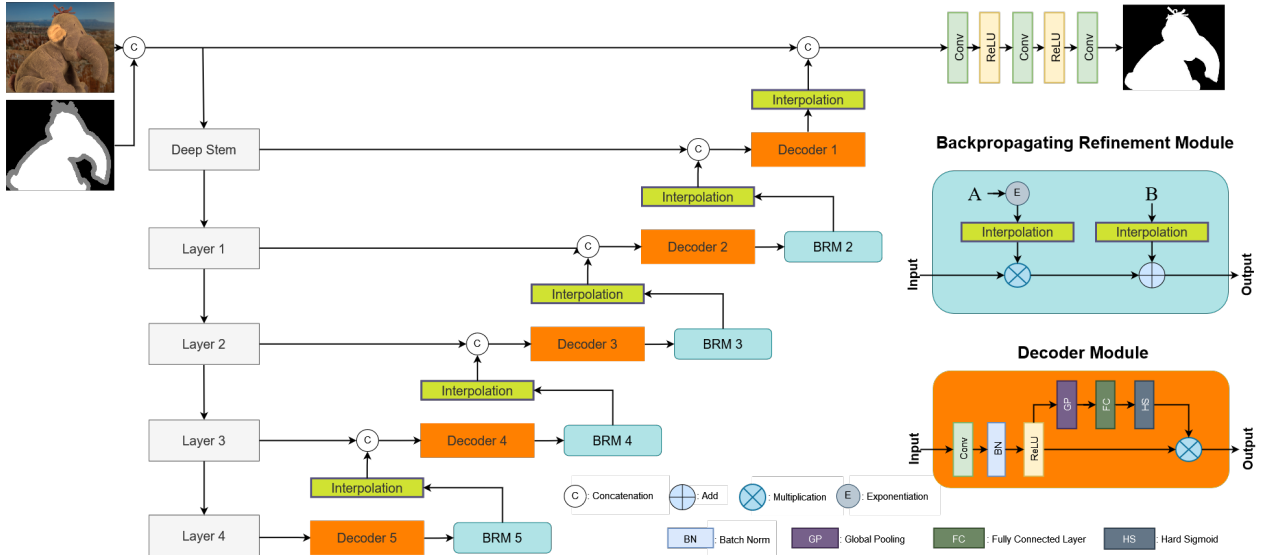


Fig. 1. Proposed network architecture.

modern deep image matting methods. We propose three techniques to guide deep image matting methods based on the local smoothness assumptions. The proposed three techniques work in the different stages of deep learning methods. We observe that the foreground images in the Adobe Image Matting (AIM) dataset [3] violate our first assumption. Hence our first technique is a training set refinement method which improves the AIM training set. The second technique is a color augmentation method which functions in the training phase. This technique can further improve the local smoothness property of the training data. The third technique is a backpropagating refinement method which functions in the inference phase. It enforces the output of the deep network to satisfy our second assumption. We conduct experiments to evaluate the effectiveness of the proposed techniques. In summary, the contributions of the present paper are as follows:

- This work is the first one to systematically explore the local smoothness assumptions in deep image matting.
- We propose three novel techniques to improve the performance of deep image matting models. In particular, we present the first deep image matting method which uses backpropagating refinement during inference.
- Based on the proposed techniques, we present a simple deep image matting model which achieves the state-of-the-art performance on the testing set of [3] among all methods trained solely on AIM dataset.

## 2. RELATED WORKS

A class of classical matting methods are based on pixel sampling. These methods sample colors from the known fore-

ground region and known background regions, and use them to estimate  $\alpha_i$  in the unknown region. Matting methods based on pixel sampling include [9–14].

Another traditional approach to the natural image matting problem is based on affinities between pixels. These methods make use of pixel similarities to propagate the alpha values from the region of  $\{i : \mathcal{T}_i = 0\} \cup \{i : \mathcal{T}_i = 1\}$  to the region of  $\{i : \mathcal{T}_i = 0.5\}$ . Poisson matting method [15] impose a model of the gradient of  $\mathcal{I}$  and  $\alpha$  and use Poisson equations to characterize the affinities between pixels. Levin *et al.* [1] proposed a color line model based on local smoothness assumptions and obtain a closed-form matting method. Chen *et al.* [16] proposed a KNN matting method which incorporates nonlocal information. Aksoy *et al.* [17] conceptualized the affinities as information flows and designed several information flows to control the way of propagation.

The deep learning method was introduced to the matting problem by Cho *et al.* [18]. Xu *et al.* [3] released a large scale matting dataset which greatly facilitated the subsequent deep learning methods for natural image matting. Lutz *et al.* [19] explored adversarial training in deep image matting. Lu *et al.* [20] designed an upsampling module for matting. Tang *et al.* [5] proposed a deep learning based sampling method. Cai *et al.* [21] disentangled the matting problem to trimap adaptation and alpha estimation. Li and Lu [4] proposed a nonlocal module to capture long-range contexts. Forte and Pitié [6] proposed a network which can simultaneously estimate  $\mathcal{F}$ ,  $\mathcal{B}$  and  $\alpha$ . Yu *et al.* [7] proposed a deep learning method to deal with images with extremely large size. Sun *et al.* [8] proposed a network which incorporates semantic classification.

Besides the deep learning methods mentioned above, there are also some deep learning methods which do not need an input trimap; see, e.g., [22, 23].

### 3. A BASELINE DEEP IMAGE MATTING MODEL

In this section, we introduce a simple deep neural network for natural image matting which serves as the baseline model.

**Network architecture.** Our network, as illustrated in Fig. 1, has a standard encoder-decoder architecture. The encoder is ResNet-50-D [24], a variant of ResNet-50 [25]. The input of the encoder is the concatenation of  $\mathcal{I}$  and  $\mathcal{T}$ , which has 4 channels. The input is  $32\times$  downsampled in the encoder. In the baseline model, the backpropagating refinement module is simply the identity operator. In the decoder, to fuse the global information of the feature map, we adopt the blocks in VoVNet [26] which are similar to the SE block [27]. Compared with the SE block, our module has only one convolution and uses the hard sigmoid which is faster than sigmoid.

**Loss function.** Xu *et al.* [3] considered the loss function

$$L(\hat{\alpha}, \alpha) = \frac{1}{\text{Card}(\{i : \mathcal{T}_i = 0.5\})} \sum_{\{i : \mathcal{T}_i = 0.5\}} \sqrt{(\hat{\alpha}_i - \alpha_i)^2 + \epsilon^2}.$$

To measure the difference of  $\hat{\alpha}$  and  $\alpha$  at different scales, we apply the above loss function at various scales of  $(\hat{\alpha}, \alpha)$  and use their weighted sum as the final loss function. Specifically, our loss function is  $\sum_{\ell=0}^4 2^{-\ell} L(\mathcal{P}^\ell(\hat{\alpha}), \mathcal{P}^\ell(\alpha))$ , where  $\mathcal{P}^\ell$  denotes the average pooling operator with kernel size  $2^\ell \times 2^\ell$  and stride  $2^\ell$ .

### 4. UTILIZING LOCAL SMOOTHNESS ASSUMPTIONS

For a position  $i$ , let  $\partial\{i\}$  denote the set of 4 surrounding positions of  $i$ . For a region  $R$ , let  $\partial R$  denote the boundary of  $R$ . Formally,  $i \in \partial R$  if and only if  $(\{i\} \cup \partial\{i\}) \cap R \neq \emptyset$  and  $(\{i\} \cup \partial\{i\}) \cap R^c \neq \emptyset$ . We consider the following two modest local smoothness assumptions.

**Assumption 1.**  $\mathcal{F}$  is locally constant at the positions

$$\{i : \alpha_i = 0\} \cup \partial\{i : \alpha_i = 0\}.$$

**Assumption 2.**  $\alpha$  is locally constant at the positions

$$\partial\{i : \mathcal{T}_i = 1\} \cup \partial\{i : \mathcal{T}_i = 0\}.$$

Assumptions 1 and 2 impose conditions on  $\mathcal{F}$  and  $\alpha$ , respectively. These assumptions are fairly weak. We can expect them to hold for general natural images. We do not impose any condition on  $\mathcal{B}$ . In fact, the background  $\mathcal{B}$  is often an unconstrained natural image in practice.

To justify Assumption 1, we note that according to the compositing equation (1), the value of  $\mathcal{F}$  in the region  $\{i : \alpha_i = 0\}$  does not affect the color of  $\mathcal{I}$ , and hence can be arbitrarily defined. However, the foreground colors in the region  $\{i : \alpha_i = 0\}$  do have impact on the training process of deep image matting model. In fact, some commonly adopted data augmentation techniques, e.g., image resizing and image rotation, rely on interpolation techniques. When interpolation

techniques are applied to  $\mathcal{F}$ , the nonsmooth colors in the region  $\{i : \alpha_i = 0\} \cup \partial\{i : \alpha_i = 0\}$  may contaminate the foreground colors in the region  $\{i : \alpha_i > 0\}$ . This phenomenon was observed by [6]. The problem of color contamination is eased by Assumption 1. In fact, under Assumption 1, for a position  $i$  in  $\{i : \alpha_i > 0\}$ , the sampling points of the interpolation method has similar foreground colors as  $i$  and hence will not contaminate the color of  $i$ .

To justify Assumption 2, we note that the trimap provided by users are often coarse. Since the trimap must be precise, the users may tend to be conservative and do not label pixels near the region  $\{i : 0 < \alpha_i < 1\}$  to be foreground or background. As a result, the pixels near the region  $\{i : \mathcal{T}_i = 1\}$  are very likely to have opacity exactly 1, and the pixels near the region  $\{i : \mathcal{T}_i = 0\}$  are very likely to have opacity exactly 0. Further, for the open matting datasets of [28] and [3], the trimaps are based on dilations of the region  $\{i : 0 < \alpha_i < 1\}$ . For these datasets, Assumption 2 holds strictly. In summary, Assumption 2 is a weak and reasonable assumption. Below we propose three techniques based on Assumptions 1 and 2 to improve deep image matting.

#### 4.1. Refining Training Set

Some commonly used data augmentation techniques in deep image matting rely on interpolation techniques. As observed by Forte and Pitié [6], when applying interpolation techniques to  $\mathcal{F}$ , the nonsmooth colors in the region  $\{i : \alpha_i = 0\} \cup \partial\{i : \alpha_i = 0\}$  may contaminate the foreground colors in the region  $\{i : \alpha_i > 0\}$ . That is, the violation of Assumption 1 results in color contamination. To ease this problem, Forte and Pitié [6] used the closed-form foreground estimation method in [1] to re-estimate the foregrounds in AIM dataset. However, The method of [1] was not designed to meet Assumption 1. We shall see that their method has suboptimal performance compared with the proposed re-estimation method.

In the training set of AIM,  $\mathcal{F}$  does not meet Assumption 1. Now we present a new method to re-estimate  $\mathcal{F}$ . Formally, the re-estimation problem is as follow: given an initial foreground  $\mathcal{F}$  and  $\alpha$ , the goal is to output a re-estimated  $\hat{\mathcal{F}}$  such that  $\hat{\mathcal{F}}$  has a similar behavior as  $\mathcal{F}$  when used to compose an image and that  $\hat{\mathcal{F}}$  satisfies Assumption 1. To meet these two requirements, we consider the following cost function:

$$C(\hat{\mathcal{F}}, \mathcal{F}) = \frac{1}{2} \sum_{i \in \{1, \dots, h\} \times \{1, \dots, w\}} \sum_{c=1}^3 \left\{ \alpha_i^2 (\hat{\mathcal{F}}_i^c - \mathcal{F}_i^c)^2 + \kappa (1 - \alpha_i)^2 \sum_{j \in \partial\{i\}} (\hat{\mathcal{F}}_i^c - \hat{\mathcal{F}}_j^c)^2 \right\},$$

where  $\kappa > 0$  is a hyperparameter. The cost  $\alpha_i^2 (\hat{\mathcal{F}}_i^c - \mathcal{F}_i^c)^2$  ensures  $\hat{\mathcal{F}}_i^c$  is close to  $\mathcal{F}_i^c$  when  $\alpha_i$  is large. On the other hand, the cost  $(1 - \alpha_i)^2 \sum_{j \in \partial\{i\}} (\hat{\mathcal{F}}_i^c - \hat{\mathcal{F}}_j^c)^2$  ensures that  $\hat{\mathcal{F}}_i^c$  is locally smooth when  $\alpha_i$  is small, which conforms Assumption

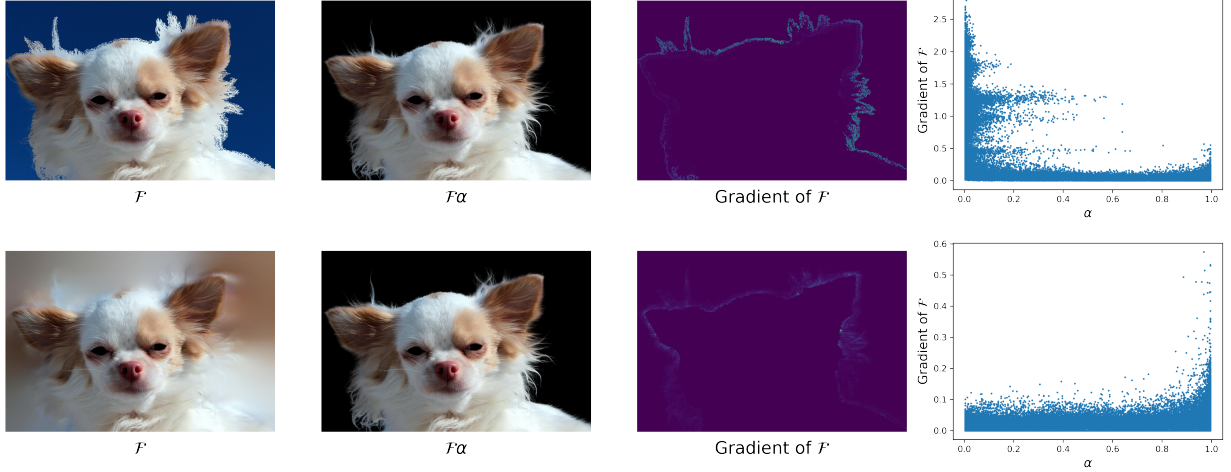


**Fig. 2.** Illustration of the effect of re-estimation of  $\mathcal{F}$ . Figures in the first row are for the original  $\mathcal{F}$ . Figures in the second row are for the re-estimated  $\mathcal{F}$ . The first column is the image  $\mathcal{F}$ . The second column is the image  $\mathcal{F}\alpha$ . The third column is the gradient of  $\mathcal{F}$ . The Fourth column is the plot of the gradient of  $\mathcal{F}$  versus  $\alpha$  within the region  $\{i : 0 < \alpha_i < 1\}$ .

1. The derivative of  $C(\hat{\mathcal{F}}, \mathcal{F})$  is

$$\frac{\partial C(\hat{\mathcal{F}}, \mathcal{F})}{\partial \hat{\mathcal{F}}_i^c} = \left( \alpha_i^2 + 4\kappa(1 - \alpha_i)^2 + \kappa \sum_{j \in \partial\{i\}} (1 - \alpha_j)^2 \right) \hat{\mathcal{F}}_i^c - \alpha_i^2 \mathcal{F}_i^c - \kappa \sum_{j \in \partial\{i\}} ((1 - \alpha_i)^2 + (1 - \alpha_j)^2) \mathcal{F}_j^c.$$

Setting the derivative  $\partial C(\hat{\mathcal{F}}, \mathcal{F}) / \partial \hat{\mathcal{F}}_i^c$  to zero yields

$$\hat{\mathcal{F}}_i^c = \frac{\alpha_i \tilde{\mathcal{I}}_i^c + \kappa \sum_{j \in \partial\{i\}} ((1 - \alpha_i)^2 + (1 - \alpha_j)^2) \mathcal{F}_j^c}{\alpha_i^2 + 4\kappa(1 - \alpha_i)^2 + \kappa \sum_{j \in \partial\{i\}} (1 - \alpha_j)^2},$$

where  $\tilde{\mathcal{I}}_i^c := \alpha_i \mathcal{F}_i^c$ . According to the above formula, a simple iteration algorithm can be obtained immediately, as summarized in Algorithm 1.

---

**Algorithm 1:** Simple Foreground Refining Algorithm

---

**Function** SimpleRefine ( $\tilde{\mathcal{I}}, \alpha, \mathcal{F}_{\text{init}}, \kappa, T$ ):

$w \leftarrow$  width of  $\mathcal{F}$ ;  $h \leftarrow$  height of  $\mathcal{F}$

$\hat{\mathcal{F}}(0) \leftarrow \mathcal{F}_{\text{init}}$

**for**  $t \leftarrow 0$  **to**  $T - 1$  **do**

**for**  $i \leftarrow 1$  **to**  $wh$  **do**

**for**  $c \leftarrow 1$  **to** 3 **do**

$$\hat{\mathcal{F}}_i^c(t+1) \leftarrow \frac{\alpha_i \tilde{\mathcal{I}}_i^c + \kappa \sum_{j \in \partial\{i\}} ((1 - \alpha_i)^2 + (1 - \alpha_j)^2) \mathcal{F}_j^c(t)}{\alpha_i^2 + 4\kappa(1 - \alpha_i)^2 + \kappa \sum_{j \in \partial\{i\}} (1 - \alpha_j)^2}$$

**return**  $\hat{\mathcal{F}}(T)$

---

In each iteration of Algorithm 1, the color in a pixel is only affected by its surrounding 4 pixels. Due to the slow speed of

---

**Algorithm 2:** Multi-Scale Foreground Refining Algorithm

---

**Input:** Foreground  $\mathcal{F}$ ; Opacity  $\alpha$ ; Scale number  $S$ ; Hyperparameter  $\kappa$ ; Iteration number  $T$ ;

$w \leftarrow$  width of  $\mathcal{F}$ ;  $h \leftarrow$  height of  $\mathcal{F}$

$\mathcal{F}_{\text{init}} \leftarrow \mathcal{F}$ ;  $\tilde{\mathcal{I}} \leftarrow \alpha \mathcal{F}$

**for**  $s \leftarrow S - 1$  **to** 0 **do**

$\tilde{\mathcal{I}}_s \leftarrow$  Resize ( $\tilde{\mathcal{I}}, 2^{-s}w, 2^{-s}h$ )

$\alpha_s \leftarrow$  Resize ( $\alpha, 2^{-s}w, 2^{-s}h$ )

$\mathcal{F}_{\text{init}} \leftarrow$  Resize ( $\mathcal{F}_{\text{init}}, 2^{-s}w, 2^{-s}h$ )

$\mathcal{F}_{\text{init}} \leftarrow$  SimpleRefine ( $\tilde{\mathcal{I}}_s, \alpha_s, \mathcal{F}_{\text{init}}, \kappa, 2^s T$ )

**return**  $\mathcal{F}_{\text{init}}$

---

foreground color propagation, Algorithm 1 may have an extremely large mixing time. Motivated by the fast multi-level foreground estimation method [29], we propose a multi-level refining procedure which first performs Algorithm 1 on the downsampled image, and gradually increases the image size to the original size. We summarize the multi-level algorithm in Algorithm 2. In practice, the parameters in Algorithm 2 are  $S = 6$ ,  $\kappa = 1$ ,  $T = 20$  and the resize operator is the bilinear interpolation.

In Fig. 2, we illustrate the effect of re-estimation of  $\mathcal{F}$  on an image in the training set of AIM [3]. It can be seen that, before re-estimation, the foreground has large variation when  $\alpha_i$  is near 0, which violates Assumption 1. After we re-estimate the foreground using the proposed algorithm, the foreground is much smoother when  $\alpha_i$  is near 0. Also, the foreground should be continuous in the region  $\{i : \alpha_i = 0\}$ .

## 4.2. Color Augmentation

In this section, we propose a simple color augmentation method to augment the training data. Given a foreground  $\mathcal{F}$ , We randomly generate an image  $\tilde{\mathcal{I}}$  with a constant color  $u$ , i.e.,  $\tilde{\mathcal{I}}_i = u$  for all  $i$ , and a random number  $w \in [0, 1]$ . The augmented foreground is defined as  $\tilde{\mathcal{F}} = w\mathcal{F} + (1-w)\tilde{\mathcal{I}}$ . To see why this simple augmentation method can work, we note that the gradient of  $\tilde{\mathcal{F}}$  is  $\nabla\tilde{\mathcal{F}} = w\nabla\mathcal{F}$ . Since  $w < 1$ , the augmented image  $\tilde{\mathcal{F}}$  is smoother than  $\mathcal{F}$ . Consequently, the augmented image is more consistent with Assumption 1.

## 4.3. Backpropagating Refinement

Now we consider the use of Assumption 2 which basically assumes that the predicted opacity  $\hat{\alpha}$  should take value 1 on  $\partial\{i : \mathcal{T}_i = 1\}$  and take value 0 on  $\partial\{i : \mathcal{T}_i = 0\}$ . Intuitively, this assumption should be satisfied by any reasonable matting methods. Surprisingly, as illustrated in the first row of Fig. 3, even for deep image matting models with good performance, the output of the network can violate Assumption 2. It shows that deep learning methods may not automatically guarantee that the known pixels annotated by the trimap has the correct result. In fact, similar phenomenon was previously observed in the field of interactive image segmentation [30, 31].

There are two possible causes of this phenomenon. First, in the training phase of most existing methods, the trimaps are obtained by dilating the regions  $\{i : \alpha_i > 0\}$  and  $\{i : \alpha_i < 1\}$ . However, such trimaps can not fully mimic the input trimap generated by users. Second, the information of sparse regions may not be fully extracted by convolutional neural networks. Specifically, suppose  $R$  is a connected component of the region  $\{i : \mathcal{T}_i = 1\}$  with a very small area. Then the important information provided by  $R$  may be very likely to be ignored by convolutional neural networks.

Given a testing image  $\mathcal{I}$  and its trimap  $\mathcal{T}$ , if the output of the deep image matting model does not satisfy Assumption 2, we would like to regulate the output to meet Assumption 2. To achieve this, the idea is to use a backpropagating procedure to refine the result during the inference phase. The use of backpropagating refinement in the inference phase has achieved great success in the interactive segmentation task [30, 31]. To the best of our knowledge, the use of backpropagating refinement in deep image matting has never been explored before.

Our backpropagating refinement method works as follows. For  $2 \leq \ell \leq 5$ , the output of Decoder  $\ell$  is processed by a Backpropagating Refinement Module (BRM) whose architecture is illustrated in Fig. 1. For BRM  $\ell$ , there are two trainable parameters  $\mathbf{A}$  and  $\mathbf{B}$  which are both tensors with dimension  $(2^{8-\ell}, 2^{8-\ell}, C)$  where  $C$  is the channel number of the input of BRM. The output of BRM is  $\exp(\mathcal{S}(\mathbf{A})) \cdot \text{Input} + \mathcal{S}(\mathbf{B})$ , where  $\mathcal{S}$  is the interpolation operator such that  $\mathcal{S}(\mathbf{A})$  and  $\mathcal{S}(\mathbf{B})$  have the same dimension as the input. In the training phase, the elements of  $\mathbf{A}$  and  $\mathbf{B}$  are fixed to 0, and hence BRM is simply the identity operator. In the inference phase, we freeze all parameters other than

the parameters in BRM. Given a testing image, we initialize the elements of  $\mathbf{A}$  and  $\mathbf{B}$  as 0 and compute the output of the network  $\hat{\alpha}_{\text{init}}$ . After that,  $\mathbf{A}$  and  $\mathbf{B}$  are iteratively updated via gradient descent to minimize the cost function

$$C_1(\hat{\alpha}, \mathcal{T}) + 0.1C_2(\hat{\alpha}, \mathcal{T}),$$

where  $\hat{\alpha}$  is the output of the network and

$$C_1(\hat{\alpha}, \mathcal{T}) = \frac{\sum_{i \in \partial\{i : \mathcal{T}_i = 0\}} \hat{\alpha}_i^2 + \sum_{i \in \partial\{i : \mathcal{T}_i = 1\}} (1 - \hat{\alpha}_i)^2}{\text{Card}(\partial\{i : \mathcal{T}_i = 0\}) + \text{Card}(\partial\{i : \mathcal{T}_i = 1\})},$$

$$C_2(\hat{\alpha}, \mathcal{T}) = \left\{ \frac{\sum_{i \in \{i : \mathcal{T}_i = 0.5\}} |\hat{\alpha}_i - \hat{\alpha}_{\text{init}, i}|}{\text{Card}(\{i : \mathcal{T}_i = 0.5\})} \right\}^2.$$

The cost function  $C_1$  regulates the output to meet Assumption 2. There may be only a small number of pixels which severely violate Assumption 2. It is known that the  $L_2$  loss is sensible to outliers. Hence in  $C_1$ , we use the  $L_2$  loss which pay more attention to the pixels that largely violate Assumption 2. On the other hand, the cost function  $C_2$  makes sure the output does not largely deviate from the original output of the network. It is known that the  $L_1$  loss is robust against a sparse set of outliers. Hence in  $C_2$ , the squared  $L_1$  loss ensures that the majority of pixels are not far away from the original output.

Note that the BRMs are all in the decoder. Hence we only need to forward the full network once and then the backward and forward computation can be restricted to the decoder. This reduces the computational cost. In practice, we set the iteration number to be 100 with learning rate 20.

## 5. EXPERIMENTS

In this section, we report experimental results of the proposed method. The source code is publicly available at <https://github.com/kfengl23/LSA-Matting>.

**Training data.** For all experiments, the encoder of the network is pretrained on ImageNet [36], and we train the network on the AIM training set [3] which consists of 431 distinct foreground images accompanied with their alpha matte and 43, 100 background images from MS-COCO dataset [37].

**Table 1.** Ablation studies on Composition-1k testing dataset. IH: input height  $h$  of training image patches. CF: closed-form foreground estimation method in [1].

IH	RF	CA	TTA	SAD	MSE	Grad	Conn
320				32.4	0.0074	11.6	29.6
480				30.0	0.0067	10.3	26.6
640				29.0	0.0062	10.3	25.4
640	CF			28.9	0.0058	10.2	25.4
640	✓			27.6	0.0057	10.1	23.6
640		✓		27.9	0.0056	9.94	23.8
640	✓	✓		25.9	0.0054	9.25	21.5
640	✓	✓	✓	<b>24.6</b>	<b>0.0045</b>	<b>8.13</b>	<b>19.9</b>

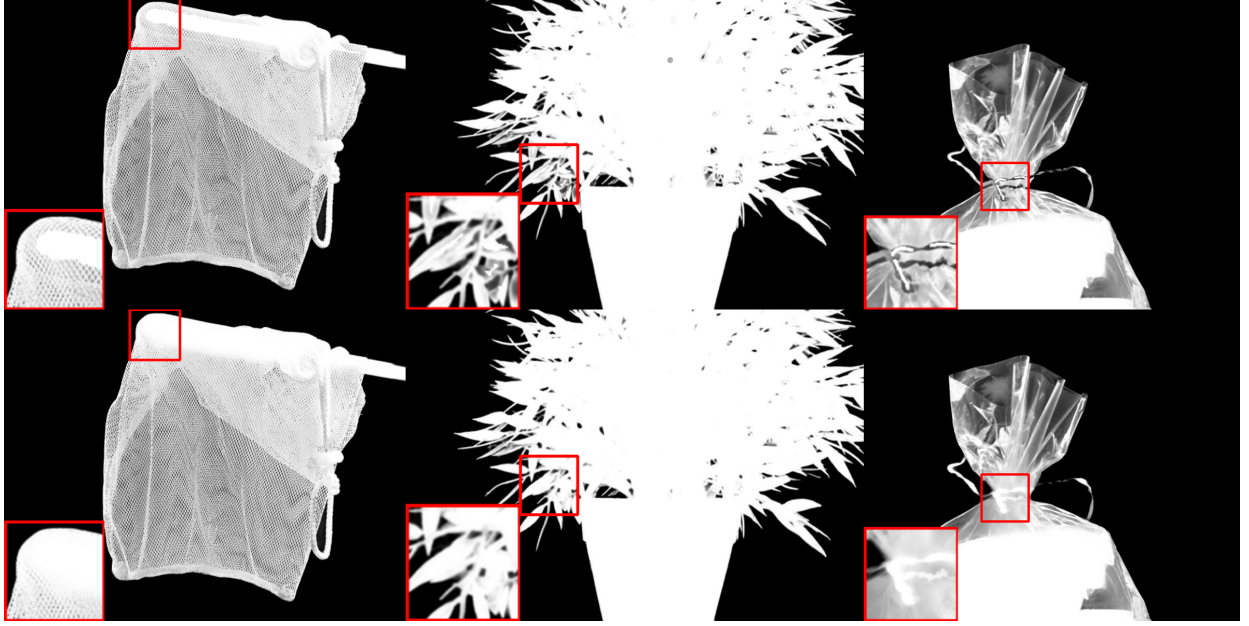


**Fig. 3.** Illustration of the effect of BR. Figures in the first row are tested without BR. Figures in the second row are tested with BR.

Sum of Absolute Differences	avg. small		avg. large		Troll (Strongly Transparent) Input			Doll (Strongly Transparent) Input			Donkey (Medium Transparent) Input			Elephant (Medium Transparent) Input			Plant (Little Transparent) Input			Pineapple (Little Transparent) Input			Plastic bag (Highly Transparent) Input			Net (Highly Transparent) Input																								
	overall rank	rank	rank	rank	small	large	user	small	large	user	small	large	user	small	large	user	small	large	user	small	large	user	small	large	user	small	large	user																						
	TransMatting	3.1	2.6	2.6	4	8.3	8.2	8.2	4.1	4.2	4.8	2.6	2.8	2.3	0.8	0.8	1.4	4.5	5.2	6.4	1.9	1.9	2.4	15.5	16.4	16.2	16.1	16.4	16.3	1																				
TMFNet	3.5	2.5	3.1	4.9	6.1	6.5	8.3	4.2	4.5	5.5	2.6	2.7	2.4	0.8	0.8	1.3	4.2	5.2	6.6	1.7	1.9	2.4	14.4	14.6	14.3	17.5	18.5	21.7	11																					
lamAlpha	4.4	5.3	4	3.9	8.4	8.4	8.4	4.4	4.4	4.4	2.7	2.7	2.7	0.9	0.9	0.9	4.8	5.2	6.2	2.5	2.7	3.1	15.8	15.8	15.8	15.9	16.5	16.5	2																					
LFPNet	4.9	4	3.8	7	7.6	8.1	9.7	4.3	4.3	5.1	3.1	3.9	2.8	0.8	0.8	1.5	3.9	4.2	5.3	1.7	1.7	2.2	17.6	18.1	17.9	16.6	16.6	17.6	3																					
TIMI-Net	5.1	6.4	5.9	3.1	8.3	8.7	9.6	4.4	4.7	4.4	2.8	2.9	2.2	1.1	1.1	1.3	4.7	5.2	6.2	1.8	1.9	2.3	15.9	16.2	15.5	16.6	19.2	18.4																						
SIM	6	6.5	5.1	6.4	8.3	8.7	9.5	4.8	4.8	6.1	2.2	2.2	2.1	0.9	0.9	1.2	4.7	5.1	6.3	2.2	2.3	2.5	15.9	16.3	16.3	17.8	18.6	20.9	8																					
PIAMatting	9.5	6.8	11.3	10.5	9.1	11	10.1	9.3	4.3	4.6	5.4	11	2.8	3.7	2.7	2.9	0.9	2.3	2.1	2.7	4.7	6.8	8.3	11	2.2	2.7	4.3	17.2	18.8	20.2	7																			
LSANet	10.3	9.9	10.9	10	8.4	9.7	8.8	4.5	5.7	5.6	3.3	3.5	3.1	1.9	1.7	1.6	5.4	7.1	8.5	2.7	3.0	3.3	17.3	17.3	16.8	16.3	17.4	21.6	10																					
HDMatt	11	12.4	9.8	10.9	9.5	13	10.2	10.7	4.7	10	4.8	5.8	15	2.9	3.8	2.6	1.1	1.4	1.2	1.3	1.3	5.2	11	5.9	6.7	2.4	2.6	3.1	17.3	10	17.3	17																		
AdaMatting	13.2	11.8	12	15.8	10.2	16	11.1	18	10.8	15	4.9	17	5.4	6.6	21	3.6	1.8	3.4	3.4	21	0.9	0.9	1.8	13	4.7	6.8	9.3	2.2	2.6	2.7	3.9	19.2	20	19.8	22	18.7	21													
A2U Matting	13.4	12.1	10.5	17.6	9.3	12	9.7	10	10.9	16	4.8	13	4.9	12	5.3	10	3.2	3.1	10	2.8	10	1.2	1.1	1.9	1.4	5.1	5.9	6.7	8.5	12	2.5	11	3.1	5.9	28	17.3	11	18.4	12	18.1	17									
SampleNet Matting	13.7	11	13.5	16.6	9.1	10	9.7	11	9.8	11	4.3	3	4.8	5.8	1	3.4	1.7	3.7	1.7	3.2	18	0.9	1.1	1.1	2.1	5.1	10	6.8	10	9.7	24	2.5	10	4.1	3.7	12	18.6	18	19.3	19	19.1	24								
FGI Matting	13.8	16.6	13.1	11.5	10.3	18	10.4	15	11.7	20	4.9	19	5.3	5.2	9	2.5	2.7	2.4	5	1.2	1.8	1.2	1.4	1.2	3	5.6	1.7	6.9	12	7.8	9	2.6	12	3.1	12	3	6	18.9	19	18.9	13	20	28	23.2	28	23.6	22	21.7	12	
GCA Matting	15	15.8	12.8	16.6	8.8	9.5	11.1	18	4.9	16	4.8	10	5.8	16	3.4	1.6	3.7	1.5	3.2	17	1.1	1.7	1.2	1.2	1.3	7	5.7	19	6.9	13	7.6	8	2.8	15	3.1	13	4.5	20	18.3	15	19.2	15	18.5	19	20.8	20	21.7	15	24.7	28

**Fig. 4.** Performance of the proposed method with BR on the AlphaMatting testing set.

No additional data is used. Instead of compositing each foreground image with a prespecified background image, we composite each foreground image with a randomly selected background in each iteration of training phase.

**Data augmentation.** Our data augmentation procedure for the baseline model is as follows. First, with probability 0.5, we randomly rotate the pair  $(\mathcal{F}, \alpha)$  and  $\mathcal{B}$ . Then we randomly crop  $(\mathcal{F}, \alpha)$  and  $\mathcal{B}$ , centered at a random pixel in the region  $\{i : \alpha > 0\}$  with size  $k \times k$  where  $k$  is randomly chosen in  $[\frac{3}{4}h, \frac{5}{4}h]$ , and then resize it to  $h \times h$  where  $h$  is the height of the input image patches in training phase. After that, with probability 0.5, we flip  $(\mathcal{F}, \alpha)$  and  $\mathcal{B}$ . With probability 0.3, we transform  $\alpha$  to  $\alpha^\gamma$  or  $1 - (1 - \alpha)^\gamma$  with equal probability where  $\gamma$  is randomly chosen in  $[0.5, 1.5]$ . With probability 0.3, we transform  $F$  to  $1 - F$ . With probability 0.3, we randomly permute the 3 channels of  $F$ . Finally, we generate the trimap by dilating the regions  $\{i : \alpha_i > 0\}$  and  $\{i : \alpha < 1\}$

by random numbers from 1 to 24.

**Implementation details.** We use Adam optimizer [38] with initial learning rate  $5 \cdot 10^{-5}$ . We halve the learning rate every 20 epochs. The model is trained for 100 epochs with batch size 16 and weight decay  $10^{-4}$ .

**Evaluation Metrics.** Following [3, 32], we use the following metrics to evaluate matting methods: the sum of absolute differences (SAD), the mean square errors (MSE), the gradient errors (Grad) and the connectivity errors (Conn).

### 5.1. Results on Composition-1k Testing Dataset

In this section, we report evaluation results on the Composition-1k testing dataset [3] to illustrate the effectiveness of two of the proposed techniques: re-estimated foregrounds (RF) and color augmentation (CA). We will evaluate the third technique in the next subsection since this technique



Sum of Absolute Differences	overall rank	avg.			Troll (Strongly Transparent) Input			Doll (Strongly Transparent) Input			Donkey (Medium Transparent) Input			Elephant (Medium Transparent) Input			Plant (Little Transparent) Input			Pineapple (Little Transparent) Input			Plastic bag (Highly Transparent) Input			Net (Highly Transparent) Input									
		small	large	user	small	large	user	small	large	user	small	large	user	small	large	user	small	large	user	small	large	user	small	large	user										
		rank	rank	rank	rank	rank	rank	rank	rank	rank	rank	rank	rank	rank	rank	rank	rank	rank	rank	rank	rank	rank	rank	rank	rank	rank									
TransMatting	3.1	2.6	2.6	4.1	8.3	8.2	8.2	4.1	4.2	4.8	2.6	2.8	2.2	0.8	0.8	1.4	4.5	5.2	6.4	1.9	1.9	2.4	15.5	16.4	16.2	16.1	16.4	16.3							
TMFNet	3.5	2.5	3	5.1	6.1	6.5	8.3	4.2	4.5	5.6	2.6	2.7	2.4	0.8	0.8	1.3	4.2	5.2	6.6	1.7	1.9	2.4	14.4	14.6	14.3	17.5	18.4	21.7							
lamAlpha	4.4	5.3	4	4	8.4	8.4	8.4	4.4	4.4	4.4	2.7	2.7	2.7	0.9	0.9	0.9	4.8	5.2	6.2	2.5	2.7	3.1	15.8	15.8	15.8	15.9	16.5	16.5							
LFPNet	4.9	3.9	3.8	7.1	7.6	8.1	9.7	4.3	4.3	5.1	3.1	3.9	2.8	0.8	0.8	1.5	3.9	4.2	5.3	1.7	1.7	2.2	17.6	18.1	17.9	16.6	16.6	17.6							
TIMI-Net	5.1	6.3	5.9	3.3	8.3	8.7	9.6	4.4	4.7	4.4	2.8	2.9	2.2	1.1	1.1	1.3	4.7	5.2	6.2	1.8	1.9	2.3	15.9	16.2	15.5	16.6	16.5	19.2							
SIM	6	6.5	5	6.5	8.3	8.7	9.5	4.8	4.8	6.1	2.2	2.2	2.1	0.9	0.9	1.1	4.7	5.1	6.3	2.2	2.3	2.5	15.9	16.3	16.3	17.8	18.5	20.9							
PIIAMatting	9.5	6.6	11.3	10.6	9.1	11	10.13	9.3	4.3	4.6	5.4	11	2.8	3.7	1.6	2.7	0.9	2.3	2.1	4.7	6.8	8.3	12	2.2	2.7	4.3	17.2	17.3	15.5						
HDMatt	11	12.1	9.8	11	9.5	13	10.12	10.7	4.7	4.9	5.8	15	2.9	3.8	2.6	1.1	1.4	1.2	1.3	5.2	5.9	6.7	2.4	2.6	3.1	17.3	17.3	17.1							
LSANet	11.3	13.4	11.8	8.6	8.5	9.7	8.8	4.7	10	5.9	20	4.9	3.3	3.5	3.2	1.9	1.7	1.1	6.6	7.8	8.2	10	2.7	3.1	3.7	17.3	10	17.4							
AdaMatting	13.2	11.8	12	15.9	10.2	16	11.1	18	10.8	15	4.9	17	5.4	1.6	6.6	21	3.6	3.4	1.2	3.4	21	0.9	0.9	1.8	4.7	6.8	9.3	2.2	2.6	3.3					
AZU Matting	13.5	12.1	10.4	17.9	9.3	12	9.7	10	10.9	16	4.8	13	4.9	12	5.3	10	3.2	3.1	10	2.8	10	1.2	1.1	1.9	1.4	5.1	6.7	8.5	2.5	3.1	5.9				
SampleNet Matting	13.7	11	13.5	16.6	9.1	10	9.7	11	9.8	11	4.3	4.8	5.1	3.4	1.7	3.2	18	0.9	1.1	1.1	2.1	5.1	10	6.8	10	9.7	24	2.5	10	4.18	3.7	12			
FGI Matting	13.8	16.5	13.1	11.6	10.3	18	10.4	15	11.7	20	4.9	19	5.3	1.5	5.2	9	2.5	2.7	2.4	5	1.2	1.8	1.4	1.2	4	5.6	16	6.9	12	7.8	2.6	12	3.1	12	3.6
GCA Matting	15	15.6	12.8	16.6	8.8	9.5	11.1	18	4.9	16	4.8	10	5.8	3.4	1.6	3.7	1.5	3.2	16	1.1	1.7	1.2	1.2	1.3	5.7	18	6.9	13	7.6	2.8	15	3.1	13	4.5	20

Fig. 5. Performance of the proposed method without BR on the AlphaMatting testing set.

Table 2. Quantitative results on Composition-1k.

Methods	SAD	MSE	Grad	Conn
Closed-form [1]	168.1	0.091	126.9	167.9
DIM [3]	50.4	0.014	31.0	50.8
IndexNet [20]	45.8	0.013	25.9	43.7
SampleNet [5]	40.4	0.0099	-	-
Context-aware [32]	35.8	0.0082	17.3	33.2
GCA [4]	35.3	0.0091	16.9	32.5
HDMatt [7]	33.5	0.0073	14.5	29.9
A <sup>2</sup> U [33]	32.2	0.0082	16.4	29.3
TIMI-Net [34]	29.1	0.0060	11.5	25.4
SIM [8]	28.0	0.0058	10.8	24.8
FBA [6]	26.4	0.0054	10.6	21.5
FBA + TTA [6]	25.8	0.0052	10.6	20.8
LFPNet [35]	23.6	0.0041	8.4	18.5
LFPNet + TTA [35]	<b>22.4</b>	<b>0.0036</b>	<b>7.6</b>	<b>17.1</b>
RF + CA (Ours)	25.9	0.0054	9.25	21.5
RF + CA + TTA (Ours)	24.6	0.0045	8.13	19.9

is time-consuming in this dataset. In addition, we also test our models with Test Time Augmentation (TTA). TTA was previously used by [5, 6] to improve the performance of the network. When TTA is used, the image is tested at three scales 0.8, 1, 1.25. For each scale, the image is rotated by  $k\pi/2$ ,  $k = 0, 1, 2, 3$ , and is flipped to generate 8 images. We run the model on these  $3 \times 8 = 24$  images and use the averaged output as the final result.

**Ablation results.** Table 1 lists the ablation results of the proposed techniques. The results indicate the following phenomena. First, while using the closed-form foreground estimation method in [1] can improve the performance, the proposed RF can lead to even better results. Second, the proposed CA can also lead to great improvement. Also, our results give quantitative characterization of the known facts that large input size in the training phase and TTA in the inference phase can lead to significant improvement of the performance.

**Comparisons with the state-of-the-art methods.** In table 2, we list the performances of some recent methods on Composition-1k. It can be seen that the methods of [35] are

the only ones whose overall performance is better than ours. However, [35] used additional data to pretrain their network. In comparison, no extra data is used in our model. Thus, our model achieves new state-of-the-art performance for all 4 metrics among all methods that are solely trained on the AIM training set.

## 5.2. Results on AlphaMatting Dataset

While our model is trained on the AIM training set, we also test our model on AlphaMatting dataset [28]. The data distribution of AlphaMatting dataset is different from AIM dataset. To increase the generalization ability of our model, we add an additional data augmentation technique in the training phase, that is, with probability 0.3, the foreground and background are blurred. Also, we train the model for 200 epochs. For all results, techniques RF, CA and TTA are used by default.

**Ablation results.** We evaluate the proposed backpropagating refinement (BR) technique on AlphaMatting training set. The results, listed in Table 3, show that BR can improve all 4 metrics. This verifies the effectiveness of BR.

**Comparisons with the state-of-the-art methods.** We evaluate the proposed method on AlphaMatting testing set. The performances of the proposed method (denoted as LSANet) and some competing methods are illustrated in Fig. 4 and Fig. 5. It can be seen that BR leads to an improvement of the ranking. While the proposed method does not rank among the top methods, it outperforms some recent methods, including [4, 5, 7, 33]. Also, the proposed method uses a simple architecture and is trained solely on AIM dataset. Overall, the performance of the proposed method is promising.

Table 3. Ablation studies on AlphaMatting training set.

Methods	SAD	MSE	Grad	Conn
Without BR	2.90	0.00540	2.47	2.45
With BR	2.87	0.00532	2.43	2.42

## 6. CONCLUSION

In this paper, we investigated the use of local smoothness assumptions in deep image matting and proposed three techniques which can improve the performance of the deep image matting model significantly. We adopted a simple network and trained the model on AIM training data. Extensive experiments verified the effectiveness of our method.

## 7. REFERENCES

- [1] Anat Levin, Dani Lischinski, and Yair Weiss, “A closed-form solution to natural image matting,” *IEEE Trans. Pattern Anal. Mach. Intell.*, vol. 30, no. 2, pp. 228–242, 2008.
- [2] Brian L. Price, Bryan S. Morse, and Scott Cohen, “Simultaneous foreground, background, and alpha estimation for image matting,” in *CVPR*, 2010, pp. 2157–2164.
- [3] Ning Xu, Brian L. Price, Scott Cohen, and Thomas S. Huang, “Deep image matting,” in *CVPR*, 2017, pp. 311–320.
- [4] Yaoyi Li and Hongtao Lu, “Natural image matting via guided contextual attention,” in *AAAI*, 2020, pp. 11450–11457.
- [5] Jingwei Tang, Yagiz Aksoy, Cengiz Öztireli, Markus H. Gross, and Tunç Ozan Aydin, “Learning-based sampling for natural image matting,” in *CVPR*, 2019, pp. 3055–3063.
- [6] Marco Forte and François Pitié, “ $F$ ,  $B$ , alpha matting,” *arXiv: 2003.07711*, 2020.
- [7] Haichao Yu, Ning Xu, Zilong Huang, Yuqian Zhou, and Humphrey Shi, “High-resolution deep image matting,” in *AAAI*, 2021, pp. 3217–3224.
- [8] Yanan Sun, Chi-Keung Tang, and Yu-Wing Tai, “Semantic image matting,” in *CVPR*, 2021, pp. 11120–11129.
- [9] Yung-Yu Chuang, Brian Curless, David Salesin, and Richard Szeliski, “A bayesian approach to digital matting,” in *CVPR*, 2001, pp. 264–271.
- [10] Jue Wang and Michael F. Cohen, “Optimized color sampling for robust matting,” in *CVPR*, 2007.
- [11] Eduardo S. L. Gastal and Manuel M. Oliveira, “Shared sampling for real-time alpha matting,” *Computer Graphics Forum*, vol. 29, no. 2, pp. 575–584, may 2010.
- [12] Kaiming He, Christoph Rhemann, Carsten Rother, Xiaoou Tang, and Jian Sun, “A global sampling method for alpha matting,” in *CVPR*, 2011, pp. 2049–2056.
- [13] Ehsan Shahrinan, Deepu Rajan, Brian L. Price, and Scott Cohen, “Improving image matting using comprehensive sampling sets,” in *CVPR*, 2013, pp. 636–643.
- [14] Xiaoxue Feng, Xiaohui Liang, and Zili Zhang, “A cluster sampling method for image matting via sparse coding,” in *ECCV*, 2016, pp. 204–219.
- [15] Jian Sun, Jiaya Jia, Chi-Keung Tang, and Heung-Yeung Shum, “Poisson matting,” *ACM Trans. Graph.*, vol. 23, no. 3, pp. 315–321, 2004.
- [16] Qifeng Chen, Dingzeyu Li, and Chi-Keung Tang, “KNN matting,” *IEEE Trans. Pattern Anal. Mach. Intell.*, vol. 35, no. 9, pp. 2175–2188, 2013.
- [17] Yagiz Aksoy, Tunç Ozan Aydin, and Marc Pollefeys, “Designing effective inter-pixel information flow for natural image matting,” *CVPR*, pp. 228–236, 2017.
- [18] Donghyeon Cho, Yu-Wing Tai, and In-So Kweon, “Natural image matting using deep convolutional neural networks,” in *ECCV*, 2016, vol. 9906, pp. 626–643.
- [19] Sebastian Lutz, Konstantinos Amplianitis, and Aljosa Smolic, “Alphagan: Generative adversarial networks for natural image matting,” in *BMVC*, 2018, p. 259.
- [20] Hao Lu, Yutong Dai, Chunhua Shen, and Songcen Xu, “Indices matter: Learning to index for deep image matting,” in *ICCV*, 2019, pp. 3265–3274.
- [21] Shaofan Cai, Xiaoshuai Zhang, Haoqiang Fan, Haibin Huang, Jiangyu Liu, Jiaming Liu, Jiaying Liu, Jue Wang, and Jian Sun, “Disentangled image matting,” in *ICCV*, 2019, pp. 8818–8827.
- [22] Soumyadip Sengupta, Vivek Jayaram, Brian Curless, Steven M. Seitz, and Ira Kemelmacher-Shlizerman, “Background matting: The world is your green screen,” in *CVPR*, 2020, pp. 2288–2297.
- [23] Yu Qiao, Yuhao Liu, Xin Yang, Dongsheng Zhou, Mingliang Xu, Qiang Zhang, and Xiaopeng Wei, “Attention-guided hierarchical structure aggregation for image matting,” in *CVPR*, 2020, pp. 13673–13682.
- [24] Tong He, Zhi Zhang, Hang Zhang, Zhongyue Zhang, Junyuan Xie, and Mu Li, “Bag of tricks for image classification with convolutional neural networks,” in *CVPR*, 2019, pp. 558–567.
- [25] Kaiming He, Xiangyu Zhang, Shaoqing Ren, and Jian Sun, “Deep residual learning for image recognition,” in *CVPR*, 2016, pp. 770–778.
- [26] Youngwan Lee, Joong-Won Hwang, Sangrok Lee, Yuseok Bae, and Jongyoul Park, “An energy and gpu-computation efficient backbone network for real-time object detection,” in *CVPRW*, 2019, pp. 752–760.
- [27] Jie Hu, Li Shen, Samuel Albanie, Gang Sun, and Enhua Wu, “Squeeze-and-excitation networks,” *IEEE Trans. Pattern Anal. Mach. Intell.*, vol. 42, no. 8, pp. 2011–2023, 2020.
- [28] Christoph Rhemann, Carsten Rother, Jue Wang, Margrit Gelautz, Pushmeet Kohli, and Pamela Rott, “A perceptually motivated online benchmark for image matting,” in *CVPR*, 2009, pp. 1826–1833.
- [29] Thomas Germer, Tobias Uelwer, Stefan Conrad, and Stefan Harmeling, “Fast multi-level foreground estimation,” in *ICPR*, 2020, pp. 1104–1111.
- [30] Won-Dong Jang and Chang-Su Kim, “Interactive image



- segmentation via backpropagating refinement scheme,” in *CVPR*, 2019, pp. 5297–5306.
- [31] Konstantin Sofiiuk, Iliia A. Petrov, Olga Barinova, and Anton Konushin, “F-BRS: rethinking backpropagating refinement for interactive segmentation,” in *CVPR*, 2020, pp. 8620–8629.
- [32] Qiqi Hou and Feng Liu, “Context-aware image matting for simultaneous foreground and alpha estimation,” in *ICCV*, 2019, pp. 4129–4138.
- [33] Yutong Dai, Hao Lu, and Chunhua Shen, “Learning affinity-aware upsampling for deep image matting,” in *CVPR*, 2021, pp. 6841–6850.
- [34] Yuhao Liu, Jiake Xie, Xiao Shi, Yu Qiao, Yujie Huang, Yong Tang, and Xin Yang, “Tripartite information mining and integration for image matting,” in *ICCV*, 2021, pp. 7555–7564.
- [35] Qinglin Liu, Haozhe Xie, Shengping Zhang, Bineng Zhong, and Rongrong Ji, “Long-range feature propagating for natural image matting,” in *ACM Multimedia*, 2021, pp. 526–534.
- [36] Jia Deng, Wei Dong, Richard Socher, Li-Jia Li, Kai Li, and Fei-Fei Li, “Imagenet: A large-scale hierarchical image database,” in *CVPR*, 2009, pp. 248–255.
- [37] Tsung-Yi Lin, Michael Maire, Serge J. Belongie, James Hays, Pietro Perona, Deva Ramanan, Piotr Dollár, and C. Lawrence Zitnick, “Microsoft COCO: common objects in context,” in *ECCV*, 2014, pp. 740–755.
- [38] Diederik P. Kingma and Jimmy Ba, “Adam: A method for stochastic optimization,” in *ICLR*, 2015.